Tuning Structure and Rheological Properties of Polyelectrolyte-Based Hydrogels through Counterion-Specific Effects

Claire Hotton, Guylaine Ducouret, Juliette Sirieix-Plénet, Thomas Bizien, Lionel Porcar, Natalie Malikova

Tuning structure and rheological properties of polyelectrolyte based hydrogels through counterion specific effects

Claire Hotton,[†] Guylaine Ducouret,[‡] Juliette Sirieix-Plénet,[†] Thomas Bizien,[¶] Lionel Porcar,[§] and Natalie Malikova*,[†]

†*Laboratory of Physical Chemistry of Electrolytes and Interfacial Nanosystems (PHENIX), Sorbonne Université, CNRS, 75005 Paris, France*

‡*Laboratory of Soft Matter Sciences and Engineering (SIMM), ESPCI Paris, PSL Research University, CNRS, F-75005 Paris, France*

¶*Synchrotron SOLEIL, l'Orme des Merisiers, Saint-Aubin - BP 48, 91192 Gif-sur-Yvette CEDEX, France*

§*Large Scale Structures, Institut Laue Langevin, Grenoble F-38042, France*

E-mail: natalie.malikova@sorbonne-universite.fr

Abstract

Tuning at will the properties of gel forming systems is of key relevance for many biotechnologies, agricultural and biomedical applications. For polyelectrolyte-based gels, ion specific effects can be an attractive way for this purpose. This study investigates the counterion specific effect on the microscopic structure and the rheological properties of a physical hydrogel formed of ionene-type cationic polyelectrolytes. The focus is on two monovalent halide counterions (F^- and Cl^-) and a divalent counterion (SO_4^{2-}). A strong counterion specific effect appears within ionene based gels. In the

case of halide counterions, gelation is more effective for more weakly hydrated counterions. Indeed, strongly hydrated counterions maintain electrostatic repulsions between the chains and as a consequence gel formation is shifted towards higher concentrations (higher critical gelation concentration, CGC). The combination of the complementary small angle X-ray and neutron scattering (SAXS, SANS) techniques reveals a strong contribution of ion-ion correlations in the structure of the gel network. Contrary to chloride gels, which present a single correlation length characterizing the distance between the cross-linking nodes, fluoride gels present an additional network of nodes. This is accompanied by a very rapid increase of the elastic modulus of fluoride gels, once CGC is reached. With divalent counterions, the gelation is even more remarkable with a lower CGC and a higher elastic modulus at equivalent polyelectrolyte concentrations. The presence of divalent counterions favours the association of chains, probably by a bridging effect. This evokes the "egg-box" model and the characteristic scaling of the elastic modulus with reduced gel concentration confirms this. However, only a narrow concentration window for gel forming exists for divalent counterions, before precipitation takes over due to too strong attractive chain-chain interactions.

Introduction

Hydrogels are a class of soft materials that have recently attracted significant attention especially for agricultural,[1] super-absorbent,[2] biotechnologies[3] and biomedical applications.[4,5] In particular, physical hydrogels which present non-permanent cross-linking bonds exhibit responsiveness to external stimuli, allowing for the control of their physicochemical properties for further applications such as drug delivery systems.[6–8] In this study, physical hydrogels are based on polyelectrolytes, i.e. charged polymers. The use of polyelectrolytes allows us to tune the hydrogel properties by changing the nature and the valence of the counterion. Here, we used ionenes, a group of cationic polyectrolyte with pH independent charge based on quaternary ammonium charged centres separated by carbon chains[9] (Figure 1 (A)).

Ionenes possess a charge density that is regular along the chain and tuneable by synthesis which enables them to be considered as a model system. While conventional ionenes do not form gel, the introduction of aromatic and amide moieties into the ionene backbone open the possibility of hydrogelation,[10,11] see Figure 1 (B). Moreover, it has been shown in the literature that these modified ionenes exhibit antimicrobial properties[12] which made these systems suitable for biomedical applications. Hydrogels based on modified ionenes are formed through a combination of electrostatic repulsions, hydrogen bonding,[10] π-π stacking, anion-π and cation-π interactions,[11,13] see Figure 1 (C).

Ion-specific effects have been investigated in the literature for many years but are still a challenging topic.[14] Ion-specificity cannot be accounted for by purely electrostatic theories, the effects of individual ions are a complex combination of their valence, polarisability, geometry and hydration properties.[14–16] Ion-specific effects on gelation mechanism have been already investigated in the literature in salty media.[17–20] Only a few studies focus on the counter-ion specific effects in non-salty media. Mostly, the effect of the valence of the counterions has been highlighted, evoking the "egg-box" model for biopolymer gels containing divalent ions.[21,22] In conventional ionene solutions, striking counterion-specific effects have already been observed[23–25] with divalent counterions but also between monovalent counterions which is quite an original feature: in this context, the chemical nature and not only the valence of the counterion could have a drastic effect on the structure and the macroscopic properties of the gel. Moreover, considering that counterion-specific effects are more pronounced for the case of positively charged chains surrounded by anions,[26,27] modified ionene based hydrogels appear to be ideal systems to explore these effects. The gel-forming ionene used is the 6-X modified ionene (6-X) represented in Figure 1 (B). The chloride counterions (X = Cl^-) are the ones obtained by synthesis. Counterion exchange is made by dialysis. Fluoride (X = F^-), another halide counterion, and a divalent counterion (X = SO_4^{2-}) are investigated here. To determine the nanoscale structure of these gels, we used a combination of small angle X-ray and neutron scattering (SAXS and SANS) techniques by taking advan-

tage of the different contrasts of the polyelectrolyte chains and the counterions available with these two beam sources, and at the same time by choosing the appropriate solvent (D_2O or H_2O). The macroscopic properties are investigated by rheological measurements.

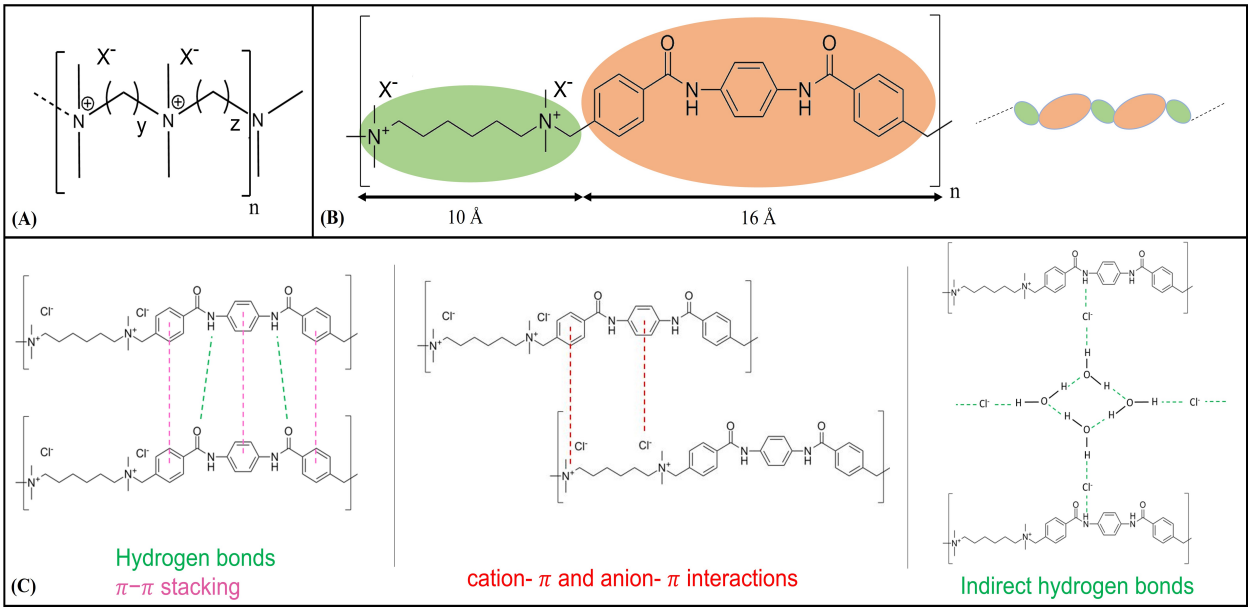

Figure 1: (A) Structure of a linear conventional ionene, y and z representing the number of methylene groups linking the charged quaternary ammonium centers. X^- represents the counterions. (B) Structure and typical lengths of the 6-X modified ionene (6 representing the number of carbons between two charged quaternary ammonium) composed of charged and aromatic blocks (in green and orange respectively). X^- represents the counterions. (C) Interchain physical interactions necessary for gel formation in the case of modified ionenes: hydrogen bonding, π-π stacking, (N^+)-π and anion-π interactions, as well as indirect hydrogen bonding via counterions and water molecules.

Experimental section

6-Cl modified ionene (6-Cl) and precursor synthesis

The 6-Cl and its precursors were synthesized by a two-step reaction with a protocol adjusted from the one described previously,[10] as detailed in.[13] The chemical reagents were all

purchased from Sigma-Aldrich and used without additional purification. The solvents were purchased from Sigma-Aldrich or VWR.

First step: synthesis of the precursor 1,4-bis-[4-(chloromethyl)ben-zamido]benzene

The vials used were all dried in an oven at 80°C 24h before use. *p*-phenylenediamine (1.08 g, 10 mmol, 1 eq) was dissolved in freshly distilled dichloromethane (100 mL) in a 250 mL round-bottom flask with a magnetic stirrer and placed under an inert argon atmosphere. The solution of *p*-phenylenediamine in the round-bottom flask was then cooled down to 0°C via an ice-water bath and triethylamine (3.5 mL, 25 mmol, 2.5 eq) was added. A solution of 4-(chloromethyl)benzoyl chloride (3.78 g, 20 mmol, 2 eq) dissolved in distilled dichloromethane (70 mL) was inserted drop-wise with an isobar dropping funnel. After the addition, the ice-water bath was removed, and the system was stirred at room temperature for 24h to ensure full conversion. The obtained white precipitate was vacuum filtrated and then washed with distilled water (2 x 80 mL). The product was dried under vacuum at 90°C. The product was obtained in high yield (85%). Structural analysis was carried out by ^{1}H-NMR in DMSO-d_6.

Second step: synthesis of 6-Cl

1,4-bis-[4-(chloromethyl)benzamido]benzene (2.06 g, 5 mmol) was dissolved in dimethylformamide (200 mL) at 80°C in a 500 mL round-bottom flask with a magnetic stirrer. N,N,N',N'-tetramethyl-1,6-hexanediamine (1.07 mL, 5 mmol) was then added. The mixture was stirred at 80°C for 48h. The obtained yellow precipitate was vacuum filtrated and washed subsequently with dimethylformamide (100 mL), acetonitrile (100 mL) and dichloromethane (100 mL). The product was dried under vacuum at 50°C. The 6-Cl was obtained in good yield (75%). Structural analysis was carried out by ^{1}H-NMR in D_2O. The average molecular weight of the 6-Cl was previously determined as 7.84 10^4 Da.[10]

Counterions exchange and formation of 6-X modified ionene hydrogels

The exchange of counterions obtained by synthesis (Cl^-) with other counterions was performed by dialysis. A solution of 6-Cl at a concentration of 0.01 M, lower than the critical gelation concentration CGC (10g/L, 0.017 M) were prepared by heating at 70°C for 10 minutes to ensure complete solubilisation of the 6-Cl in water and then cooling back to room temperature. The solution was then introduced into the dialysis cassette Slide-A-Lyzer with a cut-off of 10 kDa. The dialysis was carried out 3 times against 0.05 M of the corresponding salts (NaF or Na_2SO_4) solutions for 24h each. The excess salt was removed by 5 successive baths of ultra pure water. We checked that all the excess salt was removed by measuring the conductivity of the bath (the conductivity was equal to the one of ultra pure water after 5 successive baths). The contents of the dialysis cassette was then collected and freeze-dried to remove water.

The 6-X hydrogels were then formed by heating the 6-X modified ionene solution at 70°C (X = Cl^-, F^-) or at 90°C (X = SO_4^{2-}) for 10 minutes followed by cooling to room temperature. The CGC of the 6-X hydrogels were determined via vial inversion method and rheology measurements.

Small Angle X-ray Scattering (SAXS)

SAXS experiments were performed on the SWING beamline in SOLEIL synchrotron (Orsay, France) at a fixed energy of 16 keV. Two sample-to-detector distances of 0.5 m and 6 m were used, allowing to have a scattering wave vector (q) range of 0.002 $Å^{-1} < q < 2$ $Å^{-1}$. Cylindrical glass capillaries of 1 mm in diameter were filled with the sample in the solution state (at 70°C) and flame sealed. The hydrogels are then formed inside the capillaries by cooling down to room temperature. Two-dimensional scattering patterns were recorded on an Eiger 4M (Dectris) detector. The values of the scattering length density and the contrast

of the main components of the system will be presented later in this article. The size of the symbols of the SAXS curves reflects the errors bars. SAXS data are presented only in arbitrary units, passage to absolute units was unsactisfactory due to technical problems throughout the experiment (variations in capillary diameter).

Small Angle Neutron Scattering (SANS)

SANS experiments were performed on the D22 spectrometer at the Institute Laue-Langevin (ILL) (Grenoble, France) and on the PAXY facility at the Laboratoire Léon Brillouin (LLB) (CEA Saclay, France) under the condition of full contrast (in D_2O solvent). On the D22 spectrometer, two different sample-to-detector distances of 3 and 17 m were used. The q range available was thus 0.002 $Å^{-1}$ < q < 0.6 $Å^{-1}$. On PAXY, three different sample-to-detector distances of 1, 3 and 5 m were used together with a neutron wavelength of 4, 5 and 8.5 Å respectively. The q range available was thus 0.006 $Å^{-1}$ < q < 0.6 $Å^{-1}$. SANS measurements were carried out with samples inside quartz cells of path length of 2 mm. The values of the scattering length density and the contrast of the main components of the system will be presented later in this article.

Rheology

Rheology measurements were conducted on a strain-controlled rheometer, ARES TA instruments (LS1) equipped with a cone-plate geometry of 20 mm in diameter, an angle of 0.04 rad and a gap of 0.043 mm at 25°C. The samples were introduced into the rheometer one day after gel formation. The gel texture is not solid but rather soft and spreadable and the sample holder (plate geometry) was easily filled with the gel using a spatula. Then, the cone-plate gap was set to 0.12 mm and the excess of the sample at the edges of the cone was removed. Lastly, we fixed the gap at 0.043 mm for the measurements. We observed the presence of a slight excess of the gel at the edges which indicated a good filling of the gap. First, a short strain sweep at 1 Hz was performed to identify the linear viscoelastic plateau.

Then, a frequency sweep was performed in the linear viscoelastic regime at 1% in strain in a pulsation range from 1 to 100 rad/s. Finally, a strain sweep at 1 Hz was performed from 0.1% to 100% (ramp up) and from 100% to 0.1% (ramp down). The duration of the measurements was less than the sample drying time. When the measurement was longer, the geometry was protected by a hermetic cell to avoid the drying of the sample. Each measurement was at first repeated twice with two extracts from the same sample to check the homogeneity of the system. For the same sample the measurement from the two extracts was very reproducible (less than 2% deviation). The final data points are an average of two independent measurements for each sample (deviation between 5% and 10%). The elastic modulus values (G') are extracted from the average G' values of the flat profile in the frequency sweeps.

Results and discussion

Gelation mechanisms of modified ionene hydrogels are multiple and complex processes that have been partially described in the literature by Misawa *et al.*,[10] Yoshida *et al.*,[28] Bachl *et al.*[11] and recently by our team in a previous article.[13] The main mechanisms proposed are hydrogen bond interactions between amide groups, π-π stacking interactions and (N^+)-π cation interactions as well as electrostatic interactions. It has been assumed that hydrogen bonds between the amide functions are formed indirectly from interactions with chloride counterions and water molecules (Figure 1). The nature of counterions could thus play a predominant role in the gelation mechanism. We choose to work with two halide counterions (Cl^- and F^-) and also to compare with a divalent counterion (SO_4^{2-}).

Counterion effects on the macroscopic properties

The counterion specific effect on ionene-based gels was first investigated on macroscopic properties. For all counterions studied and for all concentrations investigated, modified ionene hydrogels exhibit a viscoelastic behaviour. In the linear domain, the elastic modulus

G' is always a decade higher than the viscous modulus G" and they are both independent of the frequency as shown in the frequency sweep in Supporting information Figure S1 (A), a typical feature of a gel. As a function of strain, the systems exhibit a linear viscoelastic plateau at low strains (less than 1% in strain) for which the modified ionene gels have an elastic behaviour (see the strain sweep and the evolution of stress as a function of strain in Supporting information Figure S1 (B)-(C)). Above a threshold stress (from 3% to 25% in strain), the modulus G' decreases sharply with deformation and becomes lower than the modulus G": the gel is destructured and flows.

The evolution of the elastic modulus G' as a function of the 6-X modified ionene concentration (C_{6-X}) in the linear domain is shown in Figure 2 (A). C_{6-X} is in moles of repeat unit presented in Figure 1 (B), each repeat unit containing two charges. We ensured that dialysis had no influence on the rheological properties of the system by performing rheology measurements on 6-Cl hydrogel with non-dialysed and dialysed 6-Cl (see the evolution of G' as a function of concentration with non-dialysed and dialysed 6-Cl in Supporting information Figure S2). The elastic modulus values overlap well for both systems. The first remarkable difference between the studied counterions is the critical gelation concentration (CGC) of the corresponding gels. The CGC is different for each counterion and evolves as follow: CGC (6-F) = 0.035 M (20 g/L) > CGC (6-Cl) = 0.017 M (10 g/L) > CGC (6-SO_4) = 0.007 M (5 g/L). Moreover, the values of G' are much higher for 6-SO_4 than for 6-Cl and 6-F at the same concentration. At 0.035 M for example, the order of magnitude of G' is $\sim$ 5000 Pa for 6-SO_4, $\sim$ 400 Pa for 6-Cl and only $\sim$ 1 Pa for 6-F. However, from 0.04 M, 6-SO_4 no longer forms a gel and precipitates, as a result of too strong attractive chain-chain interactions.

For all three counterions, the evolution of G' as a function of the 6-X concentration is described by a power law, with a different characteristic exponent for each counterion. Indeed, G' $\sim c^4$ for 6-Cl and G' $\sim c^3$ for 6-SO_4 while for 6-F, G' shows a fast increase represented by the dashed line in Figure 2 (A), between 0.035 M and 0.07 M. At 0.07 M in 6-F, a break in the slope appears. Beyond this critical point, the evolution of G' as a

function of concentration becomes as G'$\sim$ c$^{4.5}$, between 0.07 M and 0.1 M.

For systems that exhibit a sol-gel transition, it is relevant to plot the curves of the elastic modulus as a function of reduced modified ionene concentration C_{6-X} - CGC_{6-X} to describe the elastic behavior in the vicinity of the transition point[29]. Using such treatment in Figure 2 (B), the data assemble on a single master curve for monovalent counterions at high reduced concentration where G' exhibit a power law dependence[30] such as G' $\sim$ (C_{6-X} - CGC_{6-X})$^{2.6}$, whereas at low reduced concentration the G' values seems to deviate as expected in view of Figure 2 (A). The exponent of 2.6 is close to the predicted value of 2.67 correponding to a sol-gel transition where the gelation process obeys the percolation model[31–33] based on the Rouse description.[34] For the divalent counterion, the exponent of 2 is close to the predicted value of 1.94 related to the electrical network model.[31–33] Systems with structures consistent with the egg-box model (ionic cross-linking with divalent cations) have indeed been reported to follow the electrical network model in their elastic properties.[35]

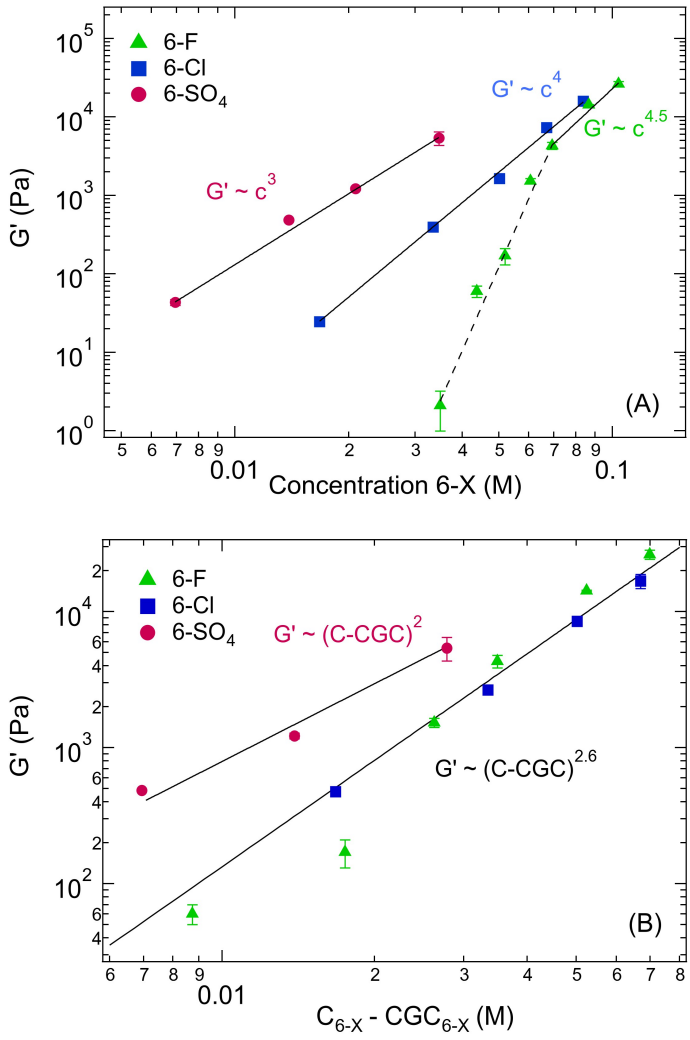

Figure 2: Evolution of the storage modulus G' of the hydrogel as a function of (A) the concentration of modified ionene C_{6-X} with different counterions and (B) the reduced concentration C_{6-X}-CGC_{6-X}, CGC being the critical gelation concentration, with different counterions.

Structure of the gel network as a function of the nature of the counterion

It is most relevant to explore now the effect of the counterions on the microscopic structure of the gels formed, in light of their very different rheological properties. Various studies have already highlighted the specific effect of counterions on the behaviour of linear conventional

ionene chains in solution. Čebaseč et al[36] showed that the enthalpies of mixing between conventional ionenes and salts can be positive or negative depending on the nature of the counterion. In the case of the fluoride counterion, the reactions are endothermic while they are exothermic with bromide. In this context, Malikova et al[23,24] have studied this effect on the structure of linear conventional ionenes in solution in the semi-dilute regime. The small angle neutron scattering study shows the presence of a correlation peak, the so-called polyelectrolyte peak, characteristic of the presence of chain-chain electrostatic repulsions in the system. The presence of more weakly hydrated, polarizable counterions (Cl^-, Br^- and I^-)[25] leads to the progressive disappearance of the correlation peak on the scattering curves when the ionene concentration is increased. Only the linear ionene with the counterion F^- preserves a well-defined polyelectrolyte peak over the same concentration range studied. Thus the disappearance of this peak is not due to a change in the concentration regime but due to a specific effect of the counterions. In the case of polarizable monovalent counterions, it is suggested that the absence of the peak is due to partial "condensation" of counterions onto the ionene backbone, leading to screening of repulsions between the chains. For the divalent counterions SO_4^{2-} and $C_2O_4^{2-}$, the absence of a polyelectrolyte peak could be due to a bridging effect of counterions between the ionene chains,[37] a phenomena already observed for others charged systems.[37–39]

The structure of the 6-Cl modified ionene solution and gel are different from the one of conventional ionene solutions as already described in a previous paper.[13] Figure 3 (A) displays the scattering intensity of a 6-Cl solution at 70°C and gel at room temperature after the heating-cooling process at 0.051 M. In the middle-q region, the scattering intensity evolves as $I \sim q^{-2}$, a typical feature for polymer systems, be it for solutions or gels.[40] At low q region, an upturn in the scattering intensity is observed which is associated with large-scale heterogeneities, very often seen for polyelectrolytes and gels.[41]

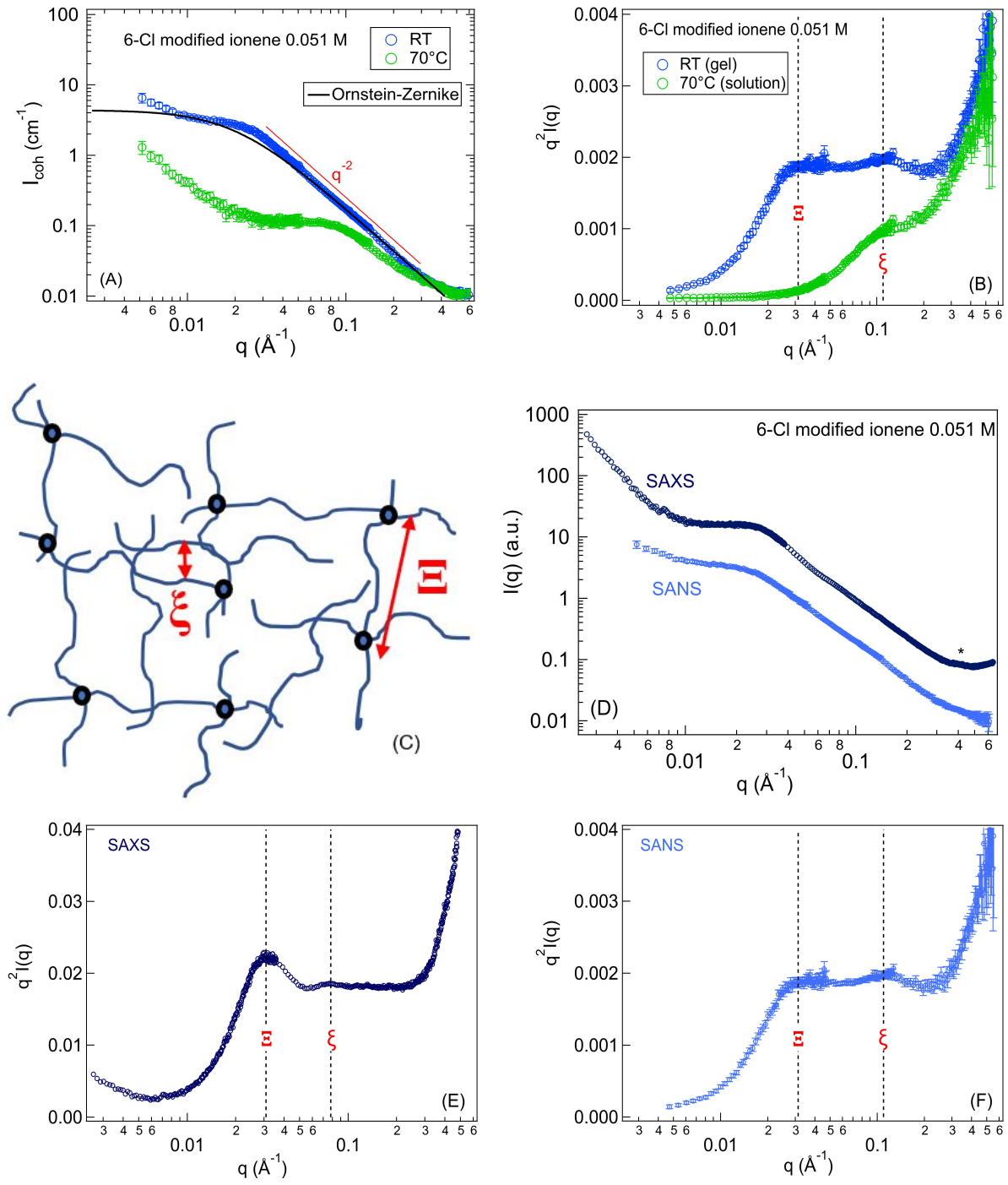

Figure 3: (A) Scattering intensity I(q) as a function of the wave vector q and (B) Kratky plots ($q^2I(q)$ as a function of the wave vector q) for the 6-Cl hydrogel (RT) and the 6-Cl solution (70°C). (C) Scheme illustrating the two characteristic lengths of the gel network. (D) Scattering intensity I(q) as a function of the wave vector q by SAXS and SANS for the 6-Cl hydrogel at 6-Cl 0.051 M. The peak marked by a star on the figure corresponds to a parasitic reflection arising from the Kapton polymer used as a window material. (E) and (F) Kratky plots by SAXS and SANS for the 6-Cl modified ionene hydrogel at 6-Cl 0.051 M.

The scattering curve of the 6-Cl gel in Figure 3 (A) presents a broad peak around 0.03 $Å^{-1}$ and a shoulder around 0.1 $Å^{-1}$. Regarding the former, it is not a well defined polyelectrolyte peak but on the other hand, the scattered intensity cannot be fully described by an Ornstein-Zernike (OZ) function ($I = \frac{I_0}{1+(q\Xi)^2}$, Ξ being the correlation length of the system)[42] which is traditionally used to describe the typical behaviour for uncharged polymer solutions and gels.[40,43,44] In other words, in this polyelectrolyte gel the electrostatic chain-chain repulsions compete with attractions between the "aromatic" blocks in the chains, leading to a "weak" polyelectrolyte behaviour. As the counterions are involved in both the electrostatic chain-chain repulsion (through screening) and in the attractive interactions (see again Figure 1 (C)), the system is indeed very sensitive to the counterion nature.

Regarding the shoulder around 0.1 $Å^{-1}$, this contribution is already present in the 6-Cl solution at high temperature, as is seen in the scattering curve in Figure 3 (A). This observation leads to the description of the scattering intensity of the gel in terms of two distinct contributions:[45] one due to thermal concentration fluctuations corresponding to the scattering intensity of the polymer solution, and an excess scattering intensity due to heterogeneities introduced by cross-linking. From this two contributions, we can extract two characteristic correlation lengths related to the polymer network in the gel. The Kratky representation displayed in Figure 3 (B) reveals in the best way the values of these correlation lengths. The first peak in the low q region, around 0.03 $Å^{-1}$ characterises the distance between the cross-linking nodes. The mesh-size of the gel due to these nodes is thus estimated as $\Xi = \frac{2\pi}{q^*} = 21$ nm, q^* being the value of the maximum of the peak. The second peak around 0.1 $Å^{-1}$ characterises the chain-chain correlation due to thermal concentration fluctuations already present in solution before gelation.[46] This correlation length is estimated as $\xi = 6$ nm. These two correlation lengths are depicted schematically in Figure 3 (C).

For this study we aimed to take advantage of both small angle X-rays and neutron scattering techniques to describe the structure of the hydrogel as a function of the nature of counterions. The scattering curves from SAXS and SANS shown in Figure 3 (D) for a 6-Cl

gel display very similar profiles (curves in arbitrary y-units). When plotting the Kratky plots $q^2I(q)$ of the SAXS and SANS curves (Figure 3 (E) and Figure 3 (F)), it can be seen that the two correlation peaks present different relative intensities. Indeed, the first correlation peak corresponding to the correlation length Ξ is much more intense in SAXS curve while the second correlation peak is better visible in SANS curve. The mesh-size of the gel Ξ is located at similar q values in SAXS and SANS curves whereas the correlation length ξ is located at lower q values by SAXS compared to SANS. This feature has already been observed in polyelectrolyte solutions and is attributed to differences in the intra-molecular interactions that can be seen between SAXS and SANS due to the different contrasts.[47] In small angle scattering, the scattered intensity I(q) by polyelectrolytes is composed of both the signal of the chains and the signal of the counterions as follows:

$$I(q) = (\Delta\rho)_m^2 S_{mm}(q) + (\Delta\rho)_c^2 S_{cc}(q) + 2(\Delta\rho)_m(\Delta\rho)_c S_{cm}(q) \quad (1)$$

Where $S_{mm}(q)$, $S_{cc}(q)$ and $S_{cm}(q)$ are respectively the monomer/monomer, counterion/counterion and counterion/monomer partial scattering functions.[37,47] Table 1 gives the contrast values of the modified ionene monomer $(\Delta\rho)_{6im}^2$, the $(\Delta\rho)_X(\Delta\rho)_{6im}$ values and the contrast values of the different counterions $(\Delta\rho)_X^2$ in heavy water (for SANS) and in light water (for SAXS). The respective contributions of the different partial scattering functions are weighted by the contrasts of the monomers and the counterions. Thus, from the contrast values it is possible to estimate the relative strength of each contribution. The relative proportions of the contrasts to the total scattering intensity for the 6-Cl gel are given in Table 2.

Table 1: Values of the contrast $(\Delta\rho^2)$ (cm^{-4}) for the 6 modified ionene monomer and the several counterions as well as the $(\Delta\rho)_X(\Delta\rho)_{6im}$ values with H_2O and D_2O in SAXS and SANS respectively.

	$(\Delta\rho)_{6im}^2$	$(\Delta\rho)_{Cl^-}^2$	$(\Delta\rho)_{F^-}^2$	$(\Delta\rho)_{SO_4^{2-}}^2$	$(\Delta\rho)_{Cl^-}(\Delta\rho)_{6im}$	$(\Delta\rho)_{F^-}(\Delta\rho)_{6im}$	$(\Delta\rho)_{SO_4^{2-}}(\Delta\rho)_{6im}$
SAXS (solvent: H_2O)	$3.8\ 10^{19}$	$1.45\ 10^{21}$	$7.45\ 10^{20}$	$7.2\ 10^{19}$	$2.3\ 10^{20}$	$1.7\ 10^{20}$	$5.2\ 10^{19}$
SANS (solvent: D_2O)	$2.5\ 10^{21}$	$1.4\ 10^{21}$	$1.3\ 10^{21}$	$2.2\ 10^{21}$	$1.9\ 10^{21}$	$1.8\ 10^{21}$	$2.35\ 10^{21}$

The scattering intensity in SAXS thus comes mainly from the contrast of the chloride

Table 2: Relative proportions of contrast to total scattering intensity in SAXS and SANS for the 6-Cl, 6-F and 6-SO_4 modified ionene hydrogels.

6-Cl	$\%(\Delta\rho)^2_{6im}$	$\%(\Delta\rho)^2_{Cl^-}$	$\%(\Delta\rho)_{Cl^-}(\Delta\rho)_{6im}$
SAXS (solvent: H_2O)	2%	75%	23%
SANS (solvent: D_2O)	33%	18%	49%

6-F	$\%(\Delta\rho)^2_{6im}$	$\%(\Delta\rho)^2_{F^-}$	$\%(\Delta\rho)_{F^-}(\Delta\rho)_{6im}$
SAXS (solvent: H_2O)	3%	67%	30%
SANS (solvent: D_2O)	33%	18%	49%

6-SO_4	$\%(\Delta\rho)^2_{6im}$	$\%(\Delta\rho)^2_{SO_4^{2-}}$	$\%(\Delta\rho)_{SO_4^{2-}}(\Delta\rho)_{6im}$
SAXS (solvent: H_2O)	18%	34%	44%
SANS (solvent: D_2O)	27%	24%	49%

counter ions with water (at 75%) while in SANS the scattered intensity comes mainly from the monomer/monomer and monomer/counter ion correlations. In SAXS, the peak corresponding to the gel mesh size Ξ is much more intense than the one corresponding to the inter-chain distance ξ. This points clearly towards the chloride counterions being heavily involved in the formation of the mesh of the gel. The correlation length ξ mainly involves monomer/monomer and monomer/counterion correlations.

The SAXS and SANS scattering intensities of the modified 6-F ionene hydrogel (0.054 M) are plotted Figure 4 (A)-(C). With fluoride counterions, three different correlation peaks are now observed: a first one around 0.027 $Å^{-1}$, a second one around 0.058 $Å^{-1}$ and a third one around 0.11 $Å^{-1}$. The third correlation peak observed in the gel is attributed to the inter-chain correlation length ξ, estimated to be around 6 nm because we observed the same correlation length in the corresponding high-temperature solution (the scattering intensity and the Kratky plot of the high-temperature solution are presented in Figure S3). Thus the first two correlation peaks are assigned to two correlation lengths Ξ_1 and Ξ_2 related to the gel mesh of 23 nm and 11 nm respectively. Comparing the SAXS and SANS Kratky plots of the same gel (Figure 4 (B)-(C)), the second correlation peak corresponding to Ξ_2 is more pronounced in SAXS than in SANS. According to Table 2, in the same way as for the chloride counterions, the scattered intensity in SAXS comes mainly from the contrast of the

fluoride counterions with water (at 67%). In SANS, the scattered intensity comes mainly from the monomer/monomer and monomer/counterion correlations. Thus, the correlation length Ξ_2 extracted from the second correlation peak is related to the F^--F^- correlation within the gel.

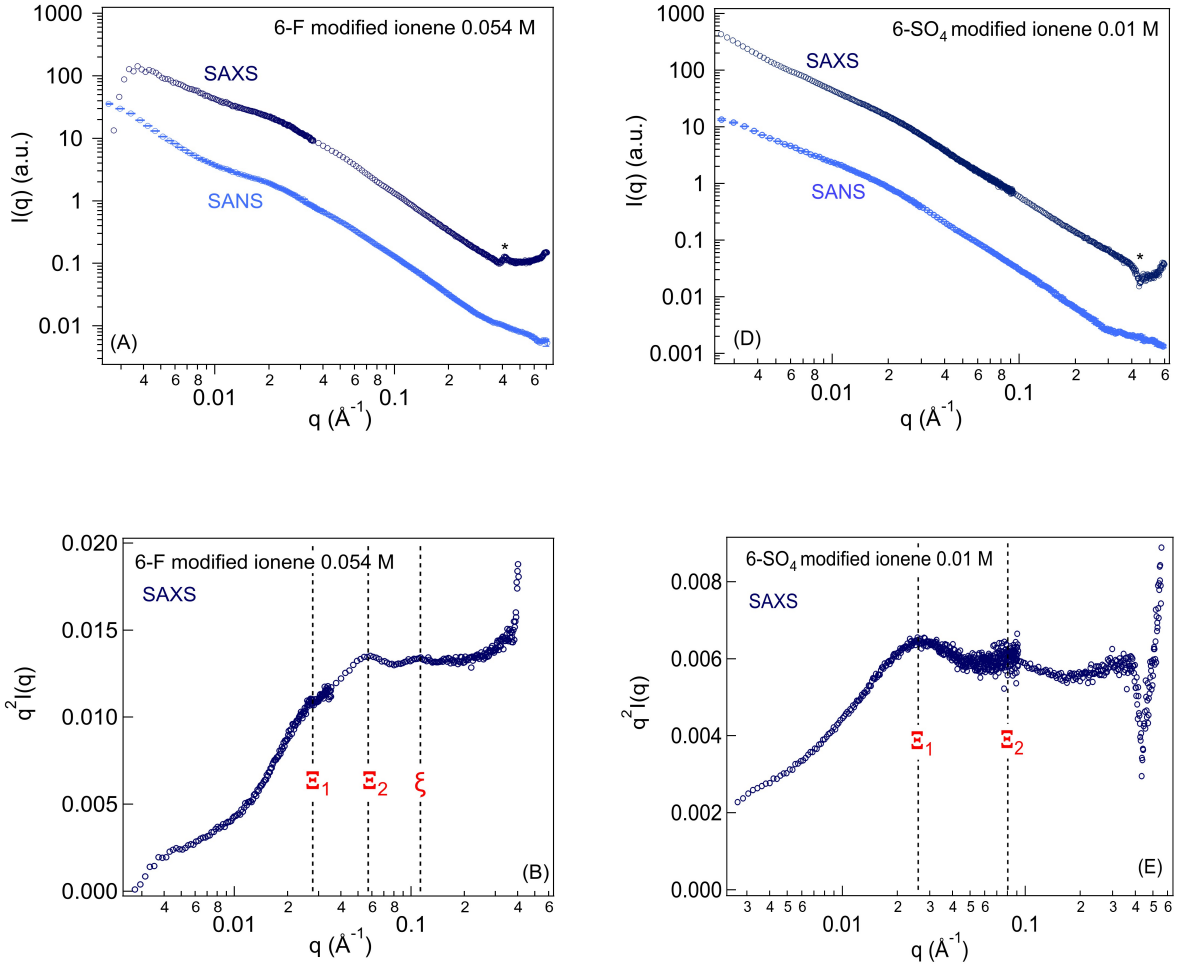

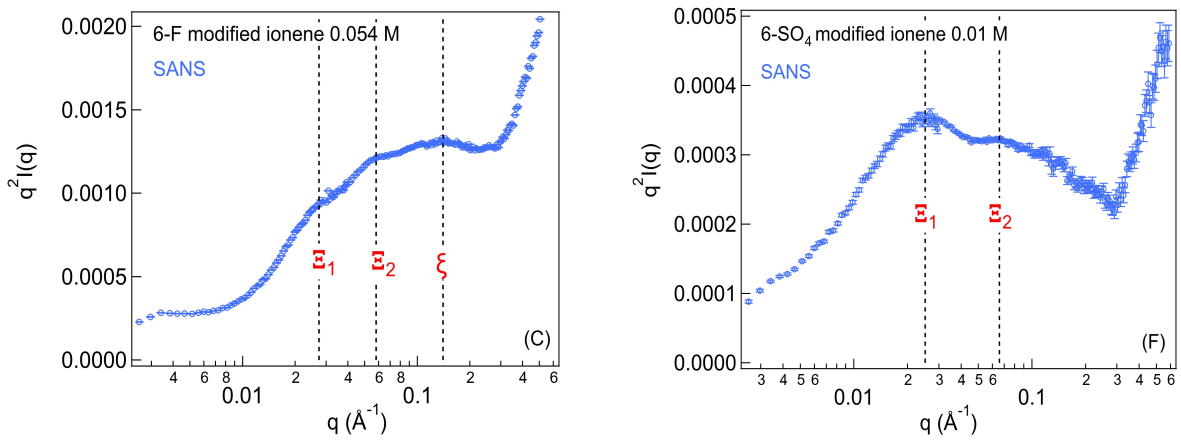

Figure 4: (A) Scattering intensity as a function of q and (B)-(C) Kratky plots ($q^2I(q)$ as a function of the wave vector q) by SAXS and SANS respectively for the 6-F modified ionene hydrogel at 0.054 M. (D) Scattering intensity as a function of q and (E)-(F) Kratky plots by SAXS and SANS respectively for the 6-SO_4 modified ionene hydrogel at 0.01 M. The peak marked by a star on the figures corresponds to a parasitic reflection arising from the Kapton polymer used as a window material.

The scattering intensities of the SAXS and SANS curves of the modified 6-SO_4 ionene gel (0.051 M) are shown in Figure 4 (D)-(F). The curves are very similar for the two scattering techniques. This is due to the fact that the relative proportions of the contrasts to the total scattering intensity are similar in SAXS and SANS (see Table 2). In the same way as for the 6-Cl gel, two correlation peaks can again be distinguished. The first peak at 0.026 Å^{-1} is attributed to the correlation length Ξ_1 estimated at 23 nm. A second peak at 0.07 Å^{-1} corresponding to a distance of 9 nm is also observed. It is difficult to determine whether this correlation peak corresponds to a distance associated with the gel mesh or to an inter-chain distance as we will see later on. We will refer to this distance as Ξ_2 in the following.

We now look at the evolution of the structure of the modified ionene gels as a function of the polyelectrolyte concentration, see Figure 5 (A) to Figure 5 (H). We observe for the 6-Cl gels that the first peak evolves towards larger q values, i.e. the gel mesh Ξ decreases when increasing the concentration of modified ionene (Figures 5 (A)-(B) and 5 (G)). The length ξ evolves with a power law as $\xi \sim c^{-0.45}$, which corresponds to the typical concentra-

tion behaviour of a polyelectrolyte solution in the semi-diluted regime[48] ($\xi \sim c^{-0.5}$ in that case) (Figure 5 (H)). The two correlation peaks become increasingly intense with increasing concentration. For 6-F gels, the longest correlation length Ξ_1 also decreases with increasing concentration as seen in Figures 5 (C)-(D) and (G). A weaker dependence is seen for Ξ_2. What is especially remarkable is that the second correlation peak related to Ξ_2 becomes increasingly more intense, as the polyelectrolyte concentration increases. The intensity evolution of the two peaks corresponding to Ξ_1 and Ξ_2 eliminates the hypothesis that these two peaks are overtones of each other. The closest picture we propose is the presence of two types of domains in the gel, corresponding to the two different Ξ. The domains with a denser mesh become dominant as the 6-F concentration increases. The length ξ follows the same trend as for the 6-Cl gels.

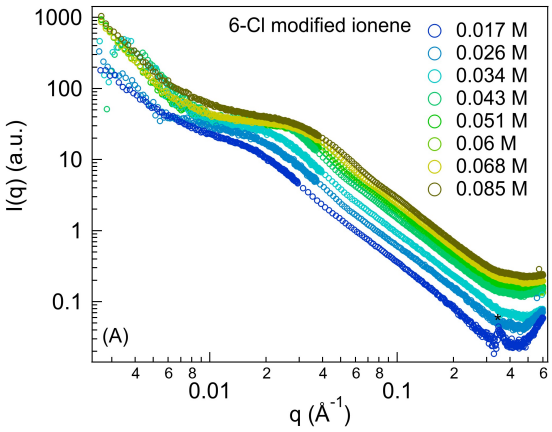
6-Cl modified ionene
0.017 M
0.026 M
0.034 M
0.043 M
0.051 M
0.06 M
0.068 M
0.085 M
I(q) (a.u.)
q (Å^{-1})
(A)

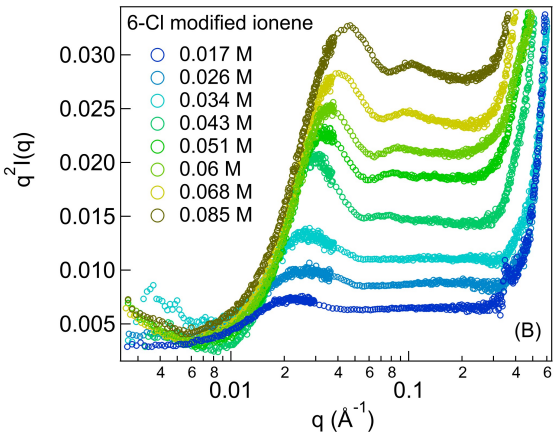
6-Cl modified ionene
0.017 M
0.026 M
0.034 M
0.043 M
0.051 M
0.06 M
0.068 M
0.085 M
q^{2}I(q)
q (Å^{-1})
(B)

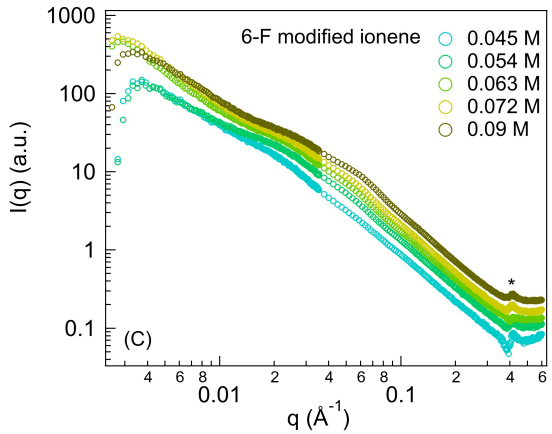
6-F modified ionene
0.045 M
0.054 M
0.063 M
0.072 M
0.09 M
I(q) (a.u.)
q (Å^{-1})
(C)

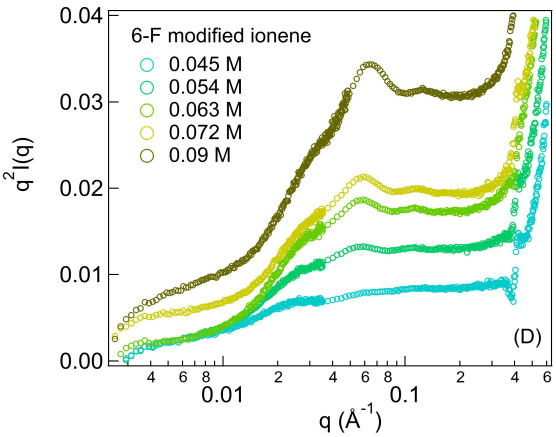
6-F modified ionene
0.045 M
0.054 M
0.063 M
0.072 M
0.09 M
q^{2}I(q)
q (Å^{-1})
(D)

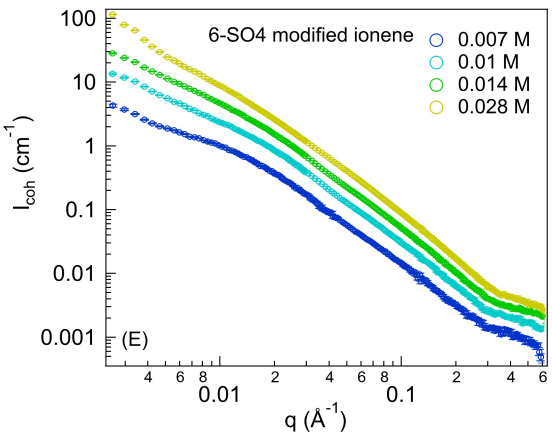
6-SO4 modified ionene
0.007 M
0.01 M
0.014 M
0.028 M
I$_{coh}$ (cm^{-1})
q (Å^{-1})
(E)

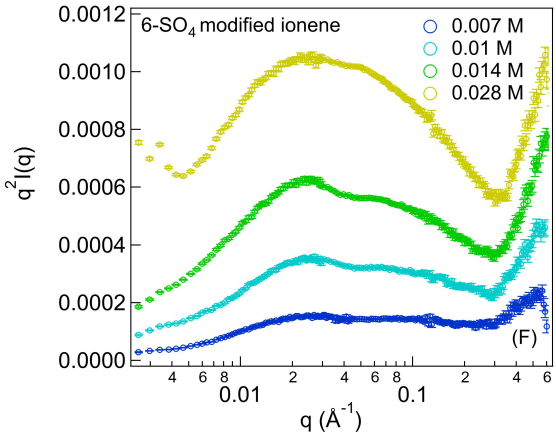
6-SO$_4$ modified ionene
0.007 M
0.01 M
0.014 M
0.028 M
q^{2}I(q)
q (Å^{-1})
(F)

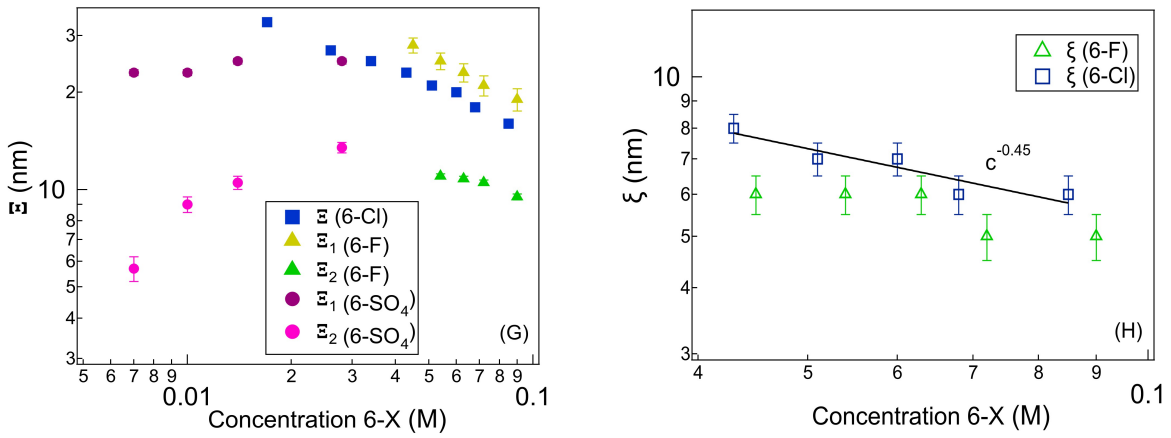

Figure 5: (A)-(F) Scattering intensity and Kratky plots ($q^2I(q)$ as a function of the wave vector q) for modified ionene hydrogels at different modified ionene concentrations by SAXS for Cl^- and F^- counterions and by SANS for SO_4^{2-} counterion. The curves (B), (D) and (F) are shifted along the y-axis for a better visualization. (G)-(H) Evolution of the gel mesh size Ξ and the inter-chain distance ξ as a function of modified ionene concentration for the three counterions studied. The peak marked by a star on the figures corresponds to a parasitic reflection arising from the Kapton polymer used as a window material.

Overall, the length Ξ_1 (6-F) is larger than the length Ξ (6-Cl) while the length Ξ_2 (6-F) is smaller than that of 6-Cl as depicted in Figure 5 (G). When concentrating the system, the smaller distance Ξ_2 within the 6-F gel mesh overrides the larger characteristic length Ξ_1. The emergence of this smaller distance could explain the rapid evolution of the elastic modulus (dashed line in Figure 2 (A)) of the 6-F gel compared to 6-Cl ($G' \sim c^4$) once the CGC of 6-F is reached, and up to 0.07 M (Figure 2 (A)). A second denser network is then present, observed only for the gel with the fluoride counterion. Beyond this critical point, the evolution of G' as a function of concentration becomes similar to that observed for the other two counterions, with $G' \sim c^{4.5}$. At the same time, we notice that the peak corresponding to Ξ_2 (6-F) starts to shift towards larger values of q. The Ξ_2 length then decreases from 11 nm to 9.5 nm. The beginning of a behaviour similar to the one of 6-Cl is then observed, i.e. a decrease of Ξ with the increase of the modified ionene concentration. To confirm this, it will be necessary to measure the scattering intensity of 6-F gels at higher concentrations of

modified ionene.

The case of 6-SO_4 gels needs to be considered apart. The SO_4-gels show a significant departure from the q^{-2} dependence in scattering intensity for the two highest concentrations compared to the gels with halide counterions, see Figure 5 (F). The strong attraction between the chains, via the bridging effect of divalent counterions (the "egg-box" model), probably leads to the formation of larger structures (contrary to a densification of a mesh). This is consistent with the concentration dependence of the second, shorter characteristic length Ξ_2, which increases with increasing concentration, unlike all other characteristic lengths presented here. Note that the larger length, Ξ_1, is constant between 25 nm and 23 nm. The "egg-box" model evokes the formation of linear, filament structures, however no q^{-1} dependence emerges in the spectra.[49] We do not have the scattering spectra of the SO_4 solutions, which would to some extent help with the assignment of the peaks and thus we do not attempt a more detailed fitting at this stage. Lastly, the strong chain-chain attraction in the case of SO_4 gels is also reflected in the appearance of syneresis when the gel is left to rest after several weeks. It is the only gel type presented here, for which syneresis is observed.

Effect of salinity

In parallel to the nature of the counterions, additional salts dramatically change the conformation of polyelectrolytes leading to the alteration of the gelation behaviour. To study the effect of salt, we form the gels in salt solutions of the same anion as their counterion by heating at 80°C and then by cooling down the system to room temperature. In 6-SO_4 gels, when 0.01 M of Na_2SO_4 salt is added, the system already precipitates, so we perform this study only for 6-Cl and 6-F gels. Figure 6 shows the scattering intensities of 6-Cl gels at 0.068 M and 6-F gels at 0.09 M upon addition of salt (NaCl and NaF respectively), and the evolution of Ξ (6-Cl) and Ξ_2 (6-F) distances in this case. For the 0.068 M 6-Cl gel, a shift in the first correlation peak, i.e. a decrease of the gel mesh size when salt is added to the system, is observed in Figure 6 (B). In addition, a disappearance of the second correlation peak is

observed. When NaF salt is added to the 0.09 M 6-F gel (Figure 6 (D)), the correlation length Ξ_2 is observed to decrease from 9.5 nm to 8 nm. Moreover, the higher the amount of salt, the more the three correlation peaks lose intensity. The addition of salt therefore has an effect on all correlation lengths of the system. As expected, the increase of the ionic strength leads to charge screening. The loss of intensity of the correlation peaks is a result of the decrease of electrostatic repulsions between the polyelectrolyte chains. The decrease in these repulsions favours the associations between the chains, cross-linking can occur more frequently and a denser mesh is observed (smaller mesh size), especially in the case of the 6-Cl gel.

The above structural changes induced by the addition of salt are reflected also in the macroscopic properties of the hydrogels. Frequency sweeps (from 1 to 100 rad/s) of hydrogels upon addition of salts show the same behavior, i.e. a fully flat G'-G" profile, as those for pure hydrogels. Is it thus possible to compare the G' values when adding salts. It is seen from Figure 7 that it leads to an increase in the elastic modulus G'. Thus, the addition of salt allows the formation of a denser network by decreasing the electrostatic repulsions between the modified ionene chains and thus favouring the attractive interactions between the chains. For the modified 6-Cl ionene gel, the G' increases up to 0.075 M in salt. From 0.1 M in NaCl, the system precipitates. For 6-F, systems with NaF additions at concentrations above 0.1 M have not been studied, but it is reasonable to assume that the system also precipitates above a certain salt concentration. Indeed, addition of salt screens the charges and when the attraction between the chains is too strong, the ionene precipitates. The F^- ions are more strongly hydrated than the Cl^- ions which explains why, compared to the 6-F gel, the 6-Cl gel strengthens over a narrower range of salt concentrations prior to precipitation.

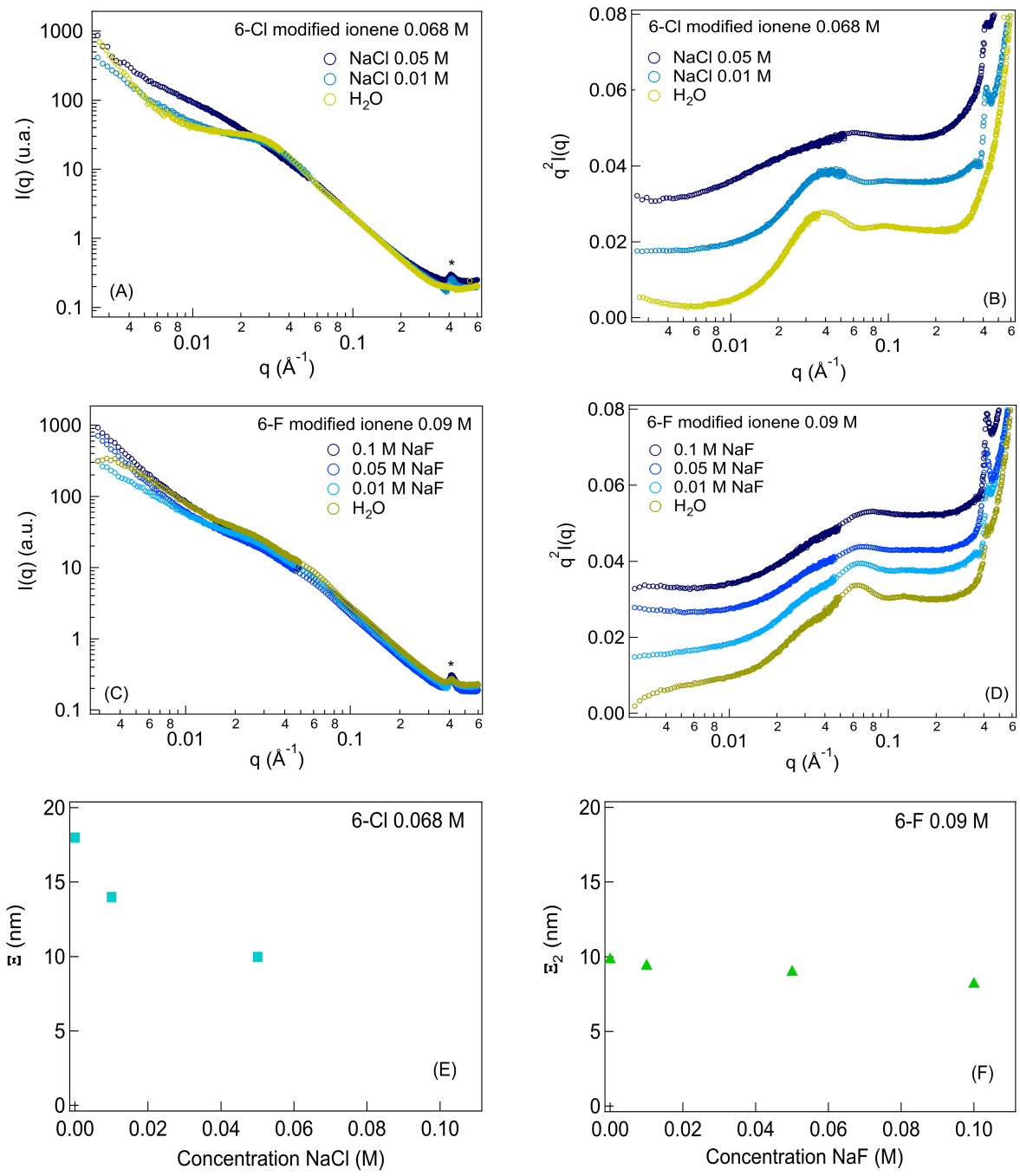

Figure 6: Scattering intensity and Kratky plots from SAXS measurements ($q^2I(q)$ as a function of the wave vector q) for (A)-(B) 6-Cl and (C)-(D) 6-F modified ionene hydrogels upon addition of salt (NaCl and NaF respectively). (E)-(F) evolution of Ξ and Ξ_2 for 6-Cl and 6-F modified ionene hydrogels upon addition of salt (NaCl and NaF respectively). The curves in (B) and (D) are shifted along the y-axis for a better visualization. The peak marked by a star on the figures corresponds to a parasitic reflection arising from the Kapton polymer used as a window material.

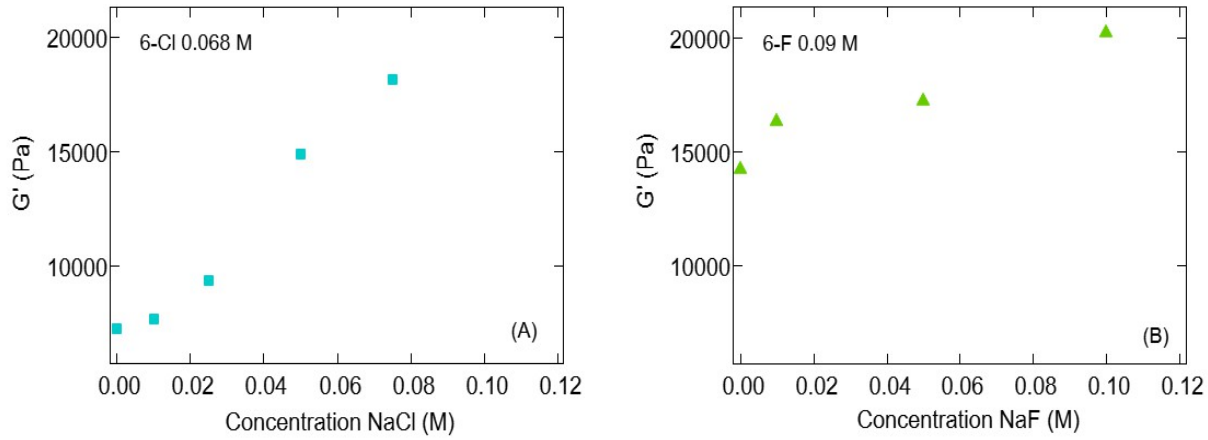

Figure 7: Evolution of the storage modulus G' of the hydrogel as a function of the concentration of (A) NaCl for 6-Cl modified ionene gel and (B) NaF for 6-F modified ionene gel.

Conclusion

Ionene-based hydrogels are formed through hydrogen bonding, π-π stacking interactions and cation-π interactions with the quaternary ammonium N^+ charged sites of the modified ionene chains and anion-π interactions with the counterions. These attractive interactions counterbalance the electrostatic repulsions between chains inherent in the presence of charged groups. This behaviour is clearly visible in the SAXS and SANS scattering curves. Indeed, the correlation peak corresponding to the characteristic distance of the gel mesh cannot be completely described either by an Ornstein Zernike function characteristic of a neutral polymer, or by a polyelectrolyte peak. The behaviour of the modified ionene chain thus results in an intermediate behaviour between that of a polyelectrolyte and that of a neutral polymer. A strong counterion specific effect exists within modified ionene hydrogels. In the case of halide counterions, gelling is less efficient when the counterions are strongly hydrated (F^-), i.e. when the ions are better dissociated from polyelectrolyte chains with a more extended counterion cloud around the chain. This extends the concentration range where chain-chain electrostatic repulsions dominate and delays the gel formation, for which

attractive chain-chain interaction are needed in order to form cross-linking nodes. The critical gelation concentration is thus higher than with a more weakly hydrated halide counterion (Cl^-). Once the critical gelation concentration is reached, a very rapid increase in the elastic modulus of the gel is observed with the fluoride counterion. In SAXS, two distances are observed characterising the mesh of 6-F gel: a larger distance than the one characterising the mesh of the 6-Cl gel and a smaller one. As the two peaks in SAXS corresponding to the two distances are not overtones (intensity evolution with concentration is inconsistent with this), two types of gel domains seem to co-exist (one related to Ξ_1 and one to Ξ_2). The domains with a denser mesh become dominant with the increase of the 6-F concentration in the gel and this correlates with a fast increase of the elastic modulus of the gel (the dashed line for 6-F as compared to G' $\sim c^4$ for 6-Cl). Once the elastic modulus reaches values similar to those of 6-Cl, the evolution of the elastic modulus of 6-F with concentration becomes similar to that of 6-Cl. In the case of divalent counterions (SO_4^{2-}), the critical gelation concentration is lower than for monovalent ions. In addition, the elastic modulus of the gel is higher than for gels with monovalent counterions at the same concentration. The presence of divalent counterions decreases electrostatic repulsions and favours the association of chains, probably by a bridging effect. On the other hand, there is a critical concentration above which the gel precipitates as a result of too strong attractive interactions between chains. The network structure of the 6-SO_4 gel seems to have two different characteristic lengths. The concentration dependence of the second (shorter) length suggests the formation of larger structures (as opposed to a densification of a mesh) in this particular system. Overall, in the reported gels, the balance between electrostatic repulsion and attractive interactions (hydrogen bonding, π-π stacking interactions and (N^+)-π cation interactions) is necessary to create cross-linking nodes and at the same time allow hydrated regions to be retained. If the electrostatic repulsion is too strong, the gel cannot form, while if the attractive interactions are too strong, the chains aggregate and the system precipitates. In conclusion, ionene-based hydrogels present a family of gels with very ion-sensitive structural and rheological

properties. At this stage, the permeability of these gels to (charged) molecular and colloidal species is a promising field of study and could pave the way to potential applications for controlled release of active substances.

Declaration of Competing Interest

The authors declare that they have no known competing financial interests or personal relationships that could have appeared to influence the work reported in this paper.

Acknowledgement

The authors thank the SOLEIL synchrotron for awarding the beamtime on beamline SWING. We would like also to acknowledge the Laboratoire Léon Brillouin for awarding the beamtime on PAXY beamline. The authors thank the Institut Laue-Langevin for the beamtime allocation on fast access (DOI: 10.5291/ILL-DATA.[86516]) for the SANS measurements. The authors thank Laurent Michot, Véronique Peyre and Jérôme Combet for fruitful discussions.

Supporting Information Available

- Supporting information. Evolution of the storage modulus and the viscous modulus as a function of the oscillation frequency and strain for the 6-X hydrogels for all counterions studied, evolution of the stress as a function of strain for the 6-X hydrogels, evolution of the storage modulus as a function of 6-Cl concentration for dialysed and non-dialysed polyelectrolyte, scattering intensity and Kratky plots for 6-F solution (80°C) and for the 6-F hydrogel (room temperature, RT).

References

(1) Qu, B.; Luo, Y. Chitosan-based hydrogel beads: Preparations, modifications and applications in food and agriculture sectors – A review. International Journal of Biological Macromolecules **2020**, 152, 437–448.

(2) Strassburg, A.; Petranowitsch, J.; Paetzold, F.; Krumm, C.; Peter, E.; Meuris, M.; Köller, M.; Tiller, J. C. Cross-Linking of a Hydrophilic, Antimicrobial Polycation toward a Fast-Swelling, Antimicrobial Superabsorber and Interpenetrating Hydrogel Networks with Long Lasting Antimicrobial Properties. ACS Applied Materials & Interfaces **2017**, 9, 36573–36582.

(3) Tavakoli, J.; Tang, Y. Hydrogel Based Sensors for Biomedical Applications: An Updated Review. Polymers **2017**, 9.

(4) Zhang, Y. S.; Khademhosseini, A. Advances in engineering hydrogels. Science **2017**, 356.

(5) Hoffman, A. S. Hydrogels for biomedical applications. Advanced Drug Delivery Reviews **2002**, 54, 3–12.

(6) Liu, Y.; Hsu, S.-h. Synthesis and Biomedical Applications of Self-healing Hydrogels. Frontiers in Chemistry **2018**, 6.

(7) Khan, M.; An, X.; Dai, L.; Li, H.; Khan, A.; Ni, Y. Chitosan-based Polymer Matrix for Pharmaceutical Excipients and Drug Delivery. Curr Med Chem **2019**, 6, 2502–2513.

(8) Suhag, D.; Bhatia, R.; Das, S.; Shakeel, A.; Ghosh, A.; Singh, A.; Sinha, O. P.; Chakrabarti, S.; Mukherjee, M. Physically cross-linked pH-responsive hydrogels with tunable formulations for controlled drug delivery. RSC Adv. **2015**, 5, 53963–5397.

(9) Noguchi, R. Reactions of N,N,N',N'-Tetramethyl–diaminoalkanes with Dihaloalkanes. Macromolecules **1972**, 5, 253–260.

(10) Misawa, Y.; Koumura, N.; Matsumoto, H.; Tamaoki, N.; Yoshida, M. Hydrogels Based on Surfactant-Free Ionene Polymers with N,N'-(p-Phenylene)dibenzamide Linkages. Macromolecules **2008**, 41, 8841–8846.

(11) Bachl, J.; Zanuy, D.; López-Pérez, D. E.; Revilla-López, G.; Cativiela, C.; Alemán, C.; Díaz, D. D. Ionene Hydrogels: Synergistic Computational-Experimental Approach to Improve Ionene Polymer-Based Functional Hydrogels. Advanced Functional Materials **2014**, 24, 4870–4870.

(12) Lou, W.; Venkataraman, S.; Zhong, G.; Ding, B.; Tan, J.; Xu, L.; Fan, W.; Yang, Y. Antimicrobial polymers as therapeutics for treatment of multidrug-resistant Klebsiella pneumoniae lung infection. Acta Biomater. **2018**, 78, 78–88.

(13) Hotton, C.; Sirieix-Plénet, J.; Ducouret, G.; Bizien, T.; Chenneviere, A.; Porcar, L.; Michot, L.; Malikova, N. Organisation of clay nanoplatelets in a polyelectrolyte-based hydrogel. J Colloid Interface Sci. **2021**, 604, 358–367.

(14) Kunz, W. Specific ion effects. World Scientific **2010**, 348.

(15) Collins, K. D. Why continuum electrostatics theories cannot explain biological structure, polyelectrolytes or ionic strength effects in ion–protein interactions. Biophysical Chemistry **2012**, 167, 43–59.

(16) Salis, A.; Ninham, B. W. Models and mechanisms of Hofmeister effects in electrolyte solutions, and colloid and protein systems revisited. Chem. Soc. Rev. **2014**, 43, 7358–7377.

(17) Qiao, C.; Wang, X.; Zhang, J.; Yao, J. Influence of salts in the Hofmeister series on the physical gelation behavior of gelatin in aqueous solutions. Food Hydrocolloids **2021**, 110, 106150.

(18) Xu, L.; Li, X.; Zhai, M.; Huang, L.; Peng, J.; Li, J.; Wei, G. Ion-Specific Swelling of Poly(styrene sulfonic acid) Hydrogel. The Journal of Physical Chemistry B **2007**, 111, 3391–3397.

(19) Roy, S.; Javid, N.; Frederix, P. W. J. M.; Lamprou, D. A.; Urquhart, A. J.; Hunt, N. T.; Halling, P. J.; Ulijn, R. V. Dramatic Specific-Ion Effect in Supramolecular Hydrogels. Chemistry – A European Journal **2012**, 18, 11723–11731.

(20) Tsai, T.-H.; Ali, M. A.; Jiang, Z.; Braun, P. V. Dynamic Gradient Directed Molecular Transport and Concentration in Hydrogel Films. Angew. Chem. Int. Ed. **2017**, 56, 5001–5006.

(21) Hu, C.; Lu, W.; Mata, A.; Nishinari, K.; Fang, Y. Ions-induced gelation of alginate: Mechanisms and applications. International Journal of Biological Macromolecules **2021**, 177, 578–588.

(22) Huynh, U. T.; Chambin, O.; Maire du Poset, A.; Assifaoui, A. Insights into gelation kinetics and gel front migration in cation-induced polysaccharide hydrogels by viscoelastic and turbidity measurements: Effect of the nature of divalent cations. Carbohydrate Polymers **2018**, 190, 121–128.

(23) Malikova, N.; Čebašek, S.; Glenisson, V.; Bhowmik, D.; Carrot, G.; Vlachy, V. Aqueous solutions of ionenes: interactions and counterion specific effects as seen by neutron scattering. Physical Chemistry Chemical Physics **2012**, 14, 12898–12904.

(24) Malikova, N.; Rollet, A.-L.; Čebašek, S.; Tomšič, M.; Vlachy, V. On the crossroads of current polyelectrolyte theory and counterion-specific effects. Physical Chemistry Chemical Physics **2015**, 17, 5650–5658.

(25) Sakhawoth, Y. Floculation - Formation et structure des agrégats entre les chaînes de polyélectrolytes et colloïdes argileux. Theses, Université Pierre et Marie Curie - Paris VI, 2017.

(26) Scheu, R.; Rankin, B. M.; Chen, Y.; Jena, K. C.; Ben-Amotz, D.; Roke, S. Charge Asymmetry at Aqueous Hydrophobic Interfaces and Hydration Shells. Angew. Chem. Int. Ed. **2014**, 53, 9560–9563.

(27) dos Santos, A. P.; Levin, Y. Ion Specificity and the Theory of Stability of Colloidal Suspensions. Phys. Rev. Lett. **2011**, 106, 167801.

(28) Yoshida, M. Ionic gelators: oligomeric and polymeric electrolytes as novel gel forming materials. The Chemical Record **2010**, 10, 230–242.

(29) Fujii, T.; Yano, T.; Kumagai, H.; Miyawaki, O. Scaling Analysis of the Concentration Dependance on Elasticity of Agarose Gel. Biosci. Biotechnol. Biochem. **2000**, 64, 1618–1622.

(30) Malo de Molina, P.; Lad, S.; Helgeson, M. E. Heterogeneity and its Influence on the Properties of Difunctional Poly(ethylene glycol) Hydrogels: Structure and Mechanics. Macromolecules **2015**, 48, 5402–5411.

(31) Vidil, T.; Cloitre, M.; Tournilhac, F. Control of Gelation and Network Properties of Cationically Copolymerized Mono- and Diglycidyl Ethers. Macromolecules, American Chemical Society **2018**, 51, 5121–5137.

(32) Stauffer, D.; Coniglio, A.; Adam, M. Gelation And Critical Phenomena. Advances in Polymer Science **1982**, 44, 103–158.

(33) Jan, N.; Coniglio, A.; Herman, H. J.; Landau, D. P.; Leyvraz, F.; Stanley, H. E. On The Relation Of Kinetic Gelation And Percolation. Journal of Physics a-Mathematical and General **1986**, 19, 399–404.

(34) Martin, J. E.; Adolf, D.; Wilcoxon, J. P. Viscoelastic Of Near-Critical Gels. Physical Review Letters **1988**, 61, 2620–2623.

(35) Suman, K.; Joshi, Y. M. On the universality of the critical scaling exponents during sol-gel transition. Materials Science **2019**, 61, 2620–2623.

(36) Čebašek, S.; Lukšič, M.; Pohar, C.; Vlachy, V. Thermodynamics of Dilution and the Hofmeister Series in Aqueous Solutions of Aliphatic Ionenes with Halide Counterions. J. Chem. Eng. Data **2011**, 56, 1282–1292.

(37) Combet, J.; Rawiso, M.; Rochas, C.; Hoffmann, S.; Boue, F. Structure of Polyelectrolytes with Mixed Monovalent and Divalent Counterions: SAXS Measurements and Poisson-Boltzmann Analysis. Macromolecules **2011**, 44, 3039–3052.

(38) Belloni, L.; Delacruz, M.; Delsanti, M.; Dalbiez, J.; Spalla, O.; Drifford, M. Polyelectrolyte Solutions Plus Multivalent Salts = Phase-Separation. Nuovo Cimento 180 Della Soc. Ital. Fis. -Condens. Matter At. Mol. Chem. Phys. Fluids Plasmas Biophys. **1994**, 16, 727–736.

(39) Dubois, E.; Boué, F. Conformation of Poly(styrenesulfonate) Polyions in the Presence of Multivalent Ions: Small-Angle Neutron Scattering Experiments. Macromolecules **2001**, 34, 3684–3697.

(40) Horkay, F.; Basser, P. J.; Hecht, A.-M.; Geissler, E. Structural investigations of a neutralized polyelectrolyte gel and an associating neutral hydrogel. Polymer **2005**, 46, 4242–4247.

(41) Shibayama, M. Small-angle neutron scattering on polymer gels: phase behavior, inhomogeneities and deformation mechanisms. Polymer Journal **2011**, 43, 18–34.

(42) Ornstein, S. L.,; Zernike, F., Accidental Deviations of Density and Opalescence at the Critical Point of a Single Substance. Proc. Acad. Sci. Amsterdam **1914**, 17, 793–806.

(43) Shibayama, M.; Ikkai, F.; Shiwa, Y.; Rabin, Y. Effect of degree of cross-linking on

spatial inhomogeneity in charged gels. I. Theoretical predictions and light scattering study. The Journal of Chemical Physics **1997**, 107, 5227–5235.

(44) Lalevée, G.; David, L.; Montembault, A.; Blanchard, K.; Meadows, J.; Malaise, S.; Crépet, A.; Grillo, I.; Morfin, I.; Delair, T.; Sudre, G. Highly stretchable hydrogels from complex coacervation of natural polyelectrolytes. Soft Matter **2017**, 13, 6594–6605.

(45) Shibayama, M. Small Angle Neutron Scattering on Gels. **2008**, 14, 783–832.

(46) Stieger, M.; Richtering, W.; Pedersen, J. S.; Lindner, P. Small-angle neutron scattering study of structural changes in temperature sensitive microgel colloids. The Journal of Chemical Physics **2004**, 120, 6197–6206.

(47) Combet, J. Structure des solutions de polyélectrolytes : apport de la diffusion des rayons X et des neutrons aux petits angles. École thématique de la Société Française de la Neutronique **2010**, 11, 153–176.

(48) De Gennes, P.; Pincus, P.; Velasco, R.; Brochard, F. Remarks on polyelectrolyte conformation. Journal de Physique **1976**, 37, 1461–1473.

(49) Li, L.; Fang, Y.; Vreeker, R.; Appelqvist, I. Reexamining the Egg-Box Model in Calcium-Alginate Gels with X-ray Diffraction. Biomacromolecules **2007**, 8, 464–468.

TOC Graphic

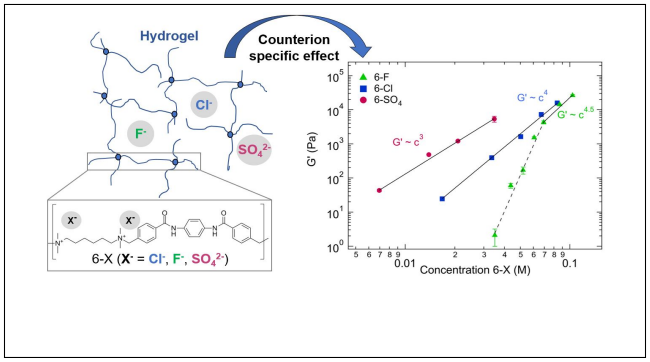
Hydrogel
Counterion
specific effect
Cl-
F-
SO4 2-
X-
X-
6-X (X- = Cl-, F-, SO4 2-)
6-F
6-Cl
6-SO4
G' ~ c3
G' ~ c4
G' ~ c4.5
G' (Pa)
Concentration 6-X (M)
0.01
0.1